

Multicode Ultra-Wideband Scheme Using Chirp Waveforms

Huaping Liu, *Member, IEEE*

Abstract—We propose an ultra-wideband (UWB) scheme that employs chirp waveforms. Signals satisfying the Federal Communications Commission (FCC) requirements for UWB applications are formed by using multiple linear frequency-modulated (chirped) waveforms. This scheme has the merits of both the multiband orthogonal frequency-division multiplexing (OFDM) UWB scheme such as continuous-wave transmission, and the pulsed UWB scheme, such as accurate timing, imaging capabilities, and rich frequency diversity. Another advantage unique to the proposed scheme is that completely passive, low-cost implementation of matched filters/correlators using surface acoustic wave devices is possible, whereas OFDM-UWB must rely on high-speed sampling combined with powerful digital signal processing. We present the details of chirp waveforms for UWB signaling, explore the correlation properties of the multICODES, and study the receiver structures. We also derive the error performance of the proposed scheme in indoor lognormal fading environments and discuss issues with the proposed scheme.

Index Terms—Chirp signals, lognormal fading channels, multicode signaling, ultra-wideband.

I. INTRODUCTION

ULTRA-WIDEBAND (UWB) has three main application areas: imaging systems (ground penetrating radar, through-wall imaging, surveillance, and medical, etc.), vehicle radar systems, and communications and measurement systems [1]. Existing UWB systems are based on one of two main approaches: pulsed scheme [2]–[7] and multiband orthogonal frequency-division multiplexing (OFDM) [8] scheme. The pulsed OFDM-UWB scheme [9] provides an improvement to the multiband OFDM scheme.

Pulsed UWB systems use pulses of short duration, typically a fraction of a nanosecond to a few nanoseconds, to transmit information. As the Federal Communications Commission (FCC) allows operation with a much higher peak power density than the average power density limit of -41.25 dBm/MHz [1], flexible tradeoff between data rate and system radio frequency (RF) coverage can be achieved by controlling the pulse repetition frequency and pulse magnitude. One of the major objectives of the OFDM-UWB scheme [8] is to improve link throughput in multipath environments. In OFDM-UWB, the 3.1–10.6-GHz spectrum for indoor UWB operations is divided into multiple subbands of 528 MHz each. Within each subband, data modulation/demodulation is realized by using OFDM.

Manuscript received March 1, 2005; revised October 15, 2005. This paper was presented in part at the IEEE MILCOM, Atlantic City, NJ, October 2005.

The author is with the School of Electrical Engineering and Computer Science, Oregon State University, Corvallis, OR 97331 USA (e-mail: hliu@eecs.oregonstate.edu).

Digital Object Identifier 10.1109/JSAC.2005.863879

The advantages and disadvantages of the existing UWB schemes are well understood [2]. The pulsed scheme has a simple transmitter, rich resolvable multipath components for multipath diversity reception, a large processing gain for robust operation in the presence of narrowband interference, and fine time resolution for accurate position location. However, multipath delay may cause severe inter-symbol interference (ISI), which ultimately limits the achievable maximum data rate. For low-data-rate applications that need a large RF coverage area, the high pulse peaks will cause problems such as power amplifier nonlinearity. Other difficulties include pulse distortion due to propagation [10], antennas [11]–[13], and other factors, making the design of a matched-filter receiver challenging. Consideration of robustness, hardware complexity, and cost often leads to conclusions that favor continuous-wave (CW) signaling for many applications.

The OFDM-UWB scheme is effective in capturing multipath energy and has a high spectral efficiency. This scheme can be efficiently implemented using FFT/IFFT. However, OFDM suffers from a number of problems, such as a high peak-to-average ratio (PAR) [8] and sensitivity to carrier frequency offset, phase noise, and timing offset. Most importantly, the multiband OFDM-UWB loses the attractive features of accurate timing and radar, as the large bandwidth is effectively divided into many small subbands.

In this paper, we explore a UWB scheme that employs linear frequency-modulated (chirped) waveforms. Linear frequency-modulated (FM) signals have historically been used extensively in radar applications. Existing research has applied linear chirp UWB signals for improved ranging [14] and for vehicle radar [15]. Recent advances in surface acoustic wave (SAW) devices have shown that generation of chirp signals and implementation of matched filter/correlators can be realized using completely passive, low-cost SAW chirp delay lines [16]–[19]. In the proposed scheme, signals satisfying the FCC requirements for UWB applications are formed by using multiple chirp waveforms. This scheme has the merits of both the multiband OFDM-UWB scheme such as CW transmission and the pulsed UWB scheme, such as accurate timing, imaging capabilities, and rich multipath diversity. The feasibility of completely passive, low-cost implementation of matched filters/correlators using SAW devices is unique to the proposed scheme. We present the details of chirp waveforms for UWB signaling, explore the correlation properties of the multICODES, and study the receiver structures. We also derive the analytical error performance of the proposed scheme in indoor multipath fading environments.

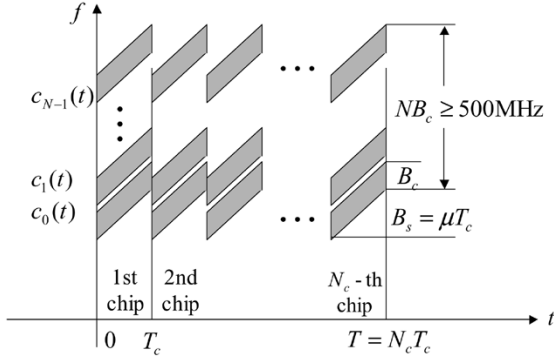


Fig. 1. Transmission scheme using multiple chirp codes.

II. ULTRA-WIDEBAND SIGNALING USING CHIRP WAVEFORMS

A. Design of Chirp Codes

We consider only linear chirp signals. To satisfy the FCC requirements for UWB operation in the 3.1–10.6 GHz, the 10-dB bandwidth of the transmitted signal must be at least 500 MHz at *all times*, or when frequency sweep is stopped [1]. The proposed scheme is illustrated in Fig. 1.

The total instantaneous bandwidth occupied by the system is divided into N subbands. Each subband is occupied by one of N waveforms $c_0(t), \dots, c_{N-1}(t)$, also called “codes” in this paper, and each code which consists of N_c chips is expressed as

$$c_n(t) = \sum_{m=0}^{N_c-1} a_{n,m} p_n \left(t - mT_c - \frac{T_c}{2} \right), \quad n = 0, \dots, N-1 \quad (1)$$

where coefficient $a_{n,m} \in \{1, -1\}$ controls the polarity of the m th chip of $c_n(t)$. Each chip of $c_n(t)$ is a linear frequency-modulated, or chirped, waveform with a duration T_c and an instantaneous bandwidth¹ B_c . Thus, the code duration is $T = N_c T_c$. The chirp waveform in each chip period of $c_n(t)$ is expressed as

$$p_n(t) = \begin{cases} g(t) \cos(2\pi(f_0 + nB_c)t + \pi\mu t^2), & |t| < \frac{T_c}{2} \\ 0, & \text{otherwise} \end{cases} \quad (2)$$

where $g(t)$ is the chirp envelope, $f_0 + nB_c$ ($f_0 \gg B_c$) is the center frequency of the n th chirp waveform, and μ is called the chirp rate. The chirp rate μ can be positive or negative; when $\mu > 0$, $p_n(t)$ is called an up-chirp; when $\mu < 0$, $p_n(t)$ is called a down-chirp. The chirp envelope $g(t)$ is a continuous-time signal with a Fourier transform $G(f)$, which is assumed to be symmetric around frequency $f = 0$ and has a bandwidth $B_c/2$. Note that the exact value of bandwidth depends on the shape of $g(t)$ and the bandwidth definition adopted (e.g., absolute bandwidth or first-null bandwidth).

¹This is at any particular time instant.

The chip coefficients $\mathbf{a}_n = [a_{n,0}, a_{n,1}, \dots, a_{n,N_c-1}]$ form the time-domain spreading sequence for the n th code $c_n(t)$. Let B_s represent the frequency-sweep range. When $B_s \gg B_c$, the total system bandwidth is mainly determined by B_s . Thus, the time-domain spreading by using sequence \mathbf{a}_n does not actually spread the signal bandwidth as in a traditional direct-sequence code-division multiple-access (CDMA) system; the instantaneous bandwidth, as well as the total bandwidth, is determined by the chip bandwidth and the frequency-sweep range. The maximum number of codes N_{\max} may be determined by the total available bandwidth, the instantaneous bandwidth, and the frequency-sweep range of each chirp.

The instantaneous frequency of $p_n(t)$ is given as

$$f_n(t) = \frac{1}{2\pi} \frac{d(2\pi(f_0 + nB_c)t + \pi\mu t^2)}{dt} = f_0 + nB_c + \mu t. \quad (3)$$

The corresponding frequency-sweep range is $B_s = |\mu|T_c$. Obviously, when frequency sweep is stopped, the instantaneous bandwidth of $p_n(t)$ is determined by the chirp envelope $g(t)$. Typical choices of $g(t)$ include $g(t) = \Pi(t/T_c)$, a rectangular window with amplitude 1 and duration T_c centered at $t = 0$, and $g(t) = \Pi(t/T_c)(1/\sqrt{2\pi}\sigma)e^{-(t^2/2\sigma^2)}$, a truncated Gaussian pulse. The choices of N and B_c must be such that $NB_c \geq 500$ MHz.

When $g(t) = \Pi(t/T_c)$, the autocorrelation function of $p_n(t)$ is given as [19] (see (4), shown at the bottom of the page). It is easy to see from (4) that although the transmitted waveforms are continuous in time, the matched filter output in the receiver has a sharp correlation peak when $B_s \gg 1$, which occurs at $t = 0$ with a value of $\sqrt{B_s T_c}$. The duration of the correlation peak [the distance in time between two zero-crossing points of $\phi_{n,n}^{(p)}(t)$] approximately equals $2/B_s$. This clearly indicates some of the major *motivations* to use the chirp signaling: the transmitted and received signals are of CW nature, but the correlation sharpness is proportional to B_s ; a larger B_s results in a sharper correlation peak in the receiver. Thus, it preserves important properties of the pulsed scheme such as accurate timing and fine multipath resolution and easy symbol synchronization through peak detection, which OFDM-UWB does not have. At the same time, CW signals make the design of hardware components, such as the power amplifier, automatic gain control, and low-noise amplifier in chirp UWB systems much easier than in pulsed systems. These properties are illustrated in Fig. 2, which compares the transmitted pulsed signals and chirp signals, as well as their autocorrelation functions.

At any particular time instant, the inner product of $p_i(t)$ and $p_j(t)$ expressed as $\int_{-T_c/2}^{T_c/2} p_i(t)p_j(t)dt, \forall i \neq j$, is always equal to zero. However, this does not imply that the cross-correlation of $p_i(t)$ and $p_j(t)$ is always zero. In fact, there might exist

$$\phi_{n,n}^{(p)}(t) = \begin{cases} \sqrt{B_s T_c} \frac{\sin\left\{\frac{\pi B_s t}{\pi B_s t} \left(1 - \frac{|t|}{T_c}\right)\right\}}{\pi B_s t} \cos(2\pi(f_0 + nB_c)t) & |t| < T_c \\ 0 & \text{otherwise.} \end{cases} \quad (4)$$

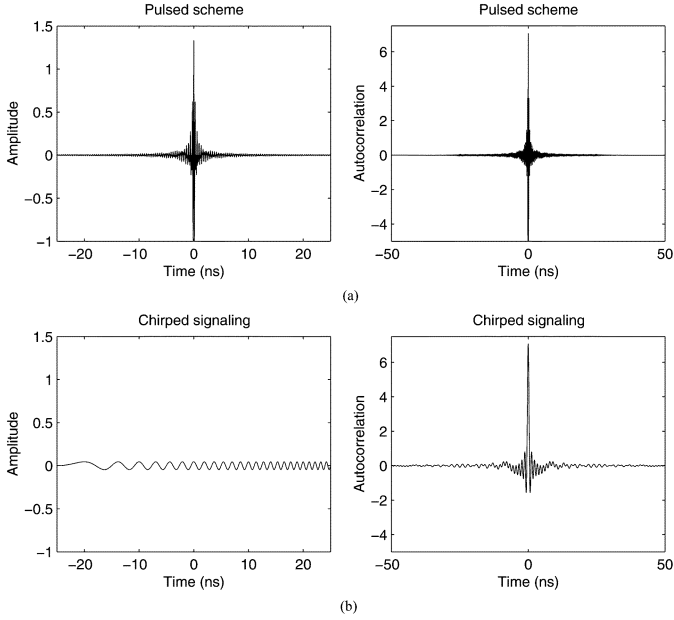


Fig. 2. Pulsed and chirp waveforms and their autocorrelation functions. (a) Top figure: pulsed waveforms. (b) Bottom figure: chirp waveforms.

a cross-correlation peak between $p_i(t)$ and $p_j(t)$, depending on the relative values of their instantaneous center frequencies and the frequency-sweep range. The time-domain spreading sequence \mathbf{a}_n must ensure that the cross-correlation values between codes $c_i(t)$ and $c_j(t)$ are as low as possible $\forall i \neq j$. Choices of \mathbf{a}_n include Walsh codes when N_c is a power of 2 and Gold codes. An example of the autocorrelation functions of $p_n(t)$ and $c_n(t)$, and the cross-correlation functions between $p_i(t)$ and $p_j(t)$, and between $c_i(t)$ and $c_j(t)$ is shown in Fig. 3. In this figure, the chip duration used is $T_c = 16$ ns, the frequency-sweep range of $p_n(t)$ adopted is $\mu T_c = 1$ GHz, and the number of chips per code applied is $N_c = 8$ with Walsh codes used as the time-domain spreading sequences for $c_n(t)$. Note that for the purpose of illustrating the autocorrelation and cross-correlation properties of $p_n(t)$ and $c_n(t)$, the energies of both signals are normalized to unity. The multiple peaks in the autocorrelation function of $c_n(t)$ when Walsh codes are used are undesirable in general. This problem can be mitigated by optimizing the spreading sequences \mathbf{a}_n so that there is *only one* dominant correlation peak.

The chirp signal $p_n(t)$ and N -chip code $c_n(t)$ discussed above have the following properties.

- 1) Let the cross-correlation between $p_i(t)$ and $p_j(t)$ be $\phi_{i,j}^{(p)}(t) = \int_{-T_c}^{T_c} p_i(\tau)p_j(t+\tau)d\tau$, $\forall i \neq j$. The chirp signals $p_n(t)$, $n = 0, \dots, N$, satisfy $\phi_{i,j}^{(p)}(0) = \phi_{i,j}^{(p)}(t)|_{t=0} = 0$, $\forall i \neq j$, $i, j = 0, \dots, N_c$. However, it does not imply that $\phi_{i,j}^{(p)}(t) = 0$ for all values of t . In fact, there might exist a value of t at which point the cross-correlation between $p_i(t)$ and $p_j(t)$ has a value approaching $\phi_{i,i}^{(p)}(0)$.
- 2) With appropriate choices of B_c , μ , \mathbf{a}_n , and $g(t)$, the N up-chirp codes $c_0(t), \dots, c_{N-1}(t)$ ($\mu > 0$) are mutually orthogonal when they are *time-aligned*. Also, $c_0(t), \dots, c_{N-1}(t)$ have small cross-correlation values.

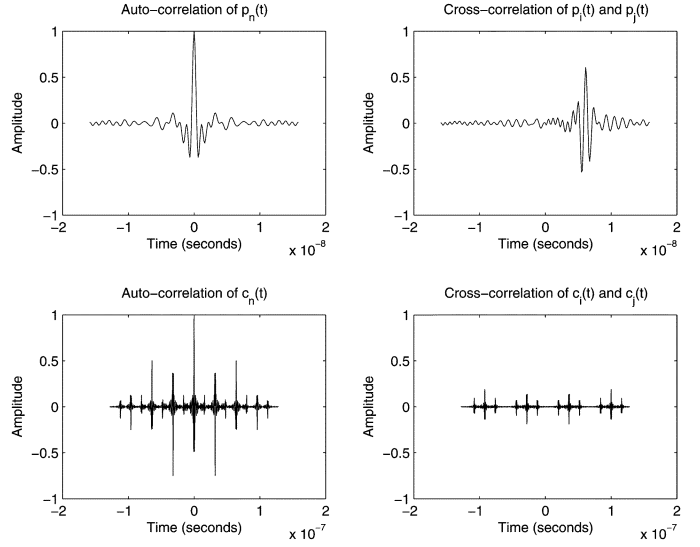


Fig. 3. Example of the autocorrelation functions of $p_n(t)$ and $c_n(t)$ (energy normalized to unity), and the cross-correlation functions between $p_i(t)$ and $p_j(t)$ (energy normalized to unity), and between $c_i(t)$ and $c_j(t)$.

The same is true for the N down-chirp codes. Let the cross-correlation function between $c_i(t)$ and $c_j(t)$ be $\phi_{i,j}^{(c)}(t) = \int_{-T}^T c_i(\tau)c_j(t+\tau)d\tau$. Mathematically, the above properties are expressed as

$$\phi_{i,j}^{(c)}(0) = \int_0^T c_i(t)c_j(t)dt = 0 \quad i \neq j \quad (5a)$$

$$\frac{\phi_{i,j}^{(c)}(t)}{\phi_{i,i}^{(c)}(0)} \rightarrow 0 \quad \forall i \neq j. \quad (5b)$$

It should be mentioned that property (5b) relies on appropriately chosen time-domain spreading sequences \mathbf{a}_n for all codes.

- 3) When $|\mu|$ is much greater than NB_c , the N down-chirp codes are quasi-orthogonal with the N up-chirp codes, which is expressed as

$$\int_0^T c_i(t; \mu > 0)c_j(t; \mu < 0)dt \approx 0 \quad \forall i, j. \quad (6)$$

Therefore, there are essentially $2N$ quasi-orthogonal chirp codes available for data modulation. Note that depending a specific design (total available bandwidth, frequency sweep-range, instantaneous bandwidth, the number chips per code, etc.), the number of time-domain spreading sequences \mathbf{a}_n satisfying the above properties may limit the maximum number of codes.

In the following discussion, we focus on a single-user scenario for which all N up-chirp codes are used for data modulation. Generalization to multiuser scenarios is straightforward; the set of quasi-orthogonal codes is partitioned into subgroups, each of which can be assigned to one user. The partition of all codes into subgroups must ensure that signals of all users satisfy the minimum instantaneous bandwidth requirements for UWB signaling. Since all codes are quasi-orthogonal with one another, the multiuser scenario is similar to the conventional direct sequence (DS) CDMA communications with a group of codes, rather than a single code, being used by one user. The strategies

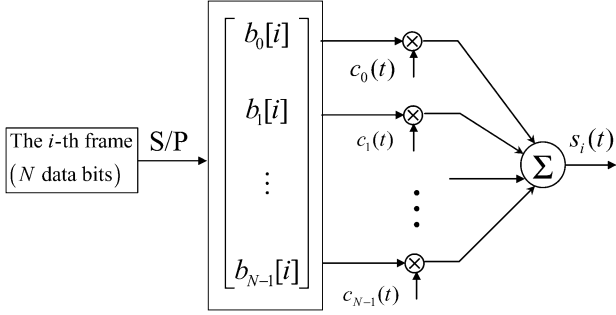


Fig. 4. Block diagram of the transmitter.

to minimize multiuser interference developed for DS-CDMA systems are directly applicable to the proposed scheme.

B. Data Modulation

We assume that the energy of all codes $c_0(t), \dots, c_{N-1}(t)$ is normalized to unity (i.e., $\int_{-\infty}^{\infty} c_n^2(t) dt = 1$) in the following discussion. We focus on binary phase-shift keying (BPSK) modulation, but the proposed scheme can be easily extended to any quadrature amplitude modulation schemes. In the baseband model, incoming bits (0s and 1s) are first nonreturn-to-zero converted. The i th frame containing N incoming data bits is serial-to-parallel converted, which then modulates the N codes, $c_1(t), \dots, c_{N-1}(t)$, forming a multicode signaling scheme. The data-modulated codes are finally summed and transmitted. The block diagram of the proposed transmitter is shown in Fig. 4.

The transmitted signal is expressed as

$$s(t) = \sum_{i=-\infty}^{\infty} s_i(t) = \sum_{i=-\infty}^{\infty} \sum_{n=0}^{N-1} \sqrt{E_b} b_n[i] c_n(t - iT) \quad (7)$$

where $s_i(t)$ is the transmitted signal in i th data frame, E_b is the energy per bit, $b_n[i] \in \{-1, 1\}$ is the n th bit of the i th frame, and $c_n(t)$ is the code given in (1). Even when frequency sweep is stopped, parameters N and B_c can be optimized to ensure that the effective instantaneous bandwidth of the transmitted signal for the i th frame given in (7) satisfies the FCC requirements for UWB signaling. The properties of $c_n(t)$ described by (5a) and (5b) ensure that $b_0[i], \dots, b_{N-1}[i]$ be separable in the receiver.

C. Receiver

Let $h_n(t)$ represent the impulse response of the channel corresponding to the n th code $c_n(t)$. Although $b_0[i]c_0(t), b_1[i]c_1(t), \dots, b_{N-1}[i]c_{N-1}(t)$ are summed, transmitted together, and arrive at the same receiver via exactly the same environment, the differences in the frequency bands they occupy may result in different fading coefficients for each of them. It is well known that the channel for pulsed UWB systems exhibits highly frequency-selective fading. Let us assume that the channel for code $c_n(t)$, $n = 0, \dots, N-1$, can be modeled as a discrete linear filter with an impulse response expressed as [20]

$$h_n(t) = \sum_{l=0}^{L-1} \alpha_{n,l} \delta(t - \tau_{n,l}) \quad (8)$$

where L is the total number of multipath components, $\alpha_{n,l}$ is the channel fading coefficient for the l th path, $\tau_{n,l}$ is the arrival time of the l th path relative to the first path ($l = 0$ and $\tau_{n,0} = 0$ assumed), and $\delta(t)$ is the Dirac delta function. Note that for simplicity, we have assumed that the total number of paths and the channel statistics (e.g., path and cluster arrival rates, cluster and path decay rates) to be defined next) for all codes are identical.

The channel gain $\alpha_{n,l}$ is modeled as $\alpha_{n,l} = \lambda_{n,l} \beta_{n,l}$, where $\lambda_{n,l}$ with an equal probability to take on the values of “−1” and “1” accounts for the random pulse inversion that could occur due to reflections [20]. The magnitude term $\beta_{n,l}$ is modeled as having a lognormal distribution for indoor channels. The standard deviation of fading amplitudes is typically in the range of 3–5 dB. The distribution of the path arrival time sequence $\tau_{n,l}$ and power delay profile of the channel are chosen to follow the modified Saleh–Valenzuela (S–V) model suggested in [20]. Because multipath components tend to arrive in clusters, $\tau_{n,l}$ in (8) is expressed as $\tau_{n,l} = \mu_c + \nu_{m,c}$, where μ_c is the delay of the c th cluster that the l th path falls in, $\nu_{m,c}$ is the delay (relative to μ_c) of the m th multipath component in the c th cluster. The relative power of the l th path to the first path can be expressed as $E\{|\alpha_{n,l}|^2\} = E\{|\alpha_{n,0}|^2\} e^{-\mu_c/\Gamma} e^{-\nu_{m,c}/\gamma}$, where $E\{\cdot\}$ denotes expectation, Γ is the cluster decay factor, and γ is the ray decay factor. Note that, different from common baseband models of narrowband systems, $\alpha_{n,l}$ is real-valued in the UWB channel model.

We will assume that linear time-invariant (LTI) system theories still apply for the chirp signaling scheme being studied in this paper. Under this condition and with the transmitted signal for the i th frame $s_i(t)$ given in (7) and the channel model (8), the received signal is expressed as

$$r_i(t) = \sum_{n=0}^{N-1} \sum_{l=0}^{L-1} \sqrt{E_b} b_n[i] \alpha_{n,l} c_n(t - iT - \tau_{n,l}) + \nu(t) \quad (9)$$

where $\nu(t)$ is the additive white Gaussian noise with a two-sided power spectral density $N_0/2$. The minimum instantaneous center frequencies between $c_i(t)$ and $c_j(t)$ could be greater than the channel coherence bandwidth. Therefore, in (9) we have assumed the general case that fading coefficients for signals $c_0(t), \dots, c_{N-1}(t)$ are different. Thus, $\alpha_{n,l}$ and $\tau_{n,l}$ are specific for each code $c_n(t)$.

One of the major differences between the chirp scheme being studied and the conventional direct-sequence spread-spectrum communication is that the frequency band of $c_n(t)$ could change significantly over each bit duration T . The received signal model given in (9) should be valid when the frequency-sweep range is not greater than the channel coherence bandwidth. However, when the frequency-sweep range is significantly larger than the channel coherence bandwidth, the channel coefficients $\{\alpha_{n,l}\}$ at different times *within the same bit interval* could be different. In this case, whether or not the LTI system theory can still be applied directly in the analysis needs further study.

As shown in Fig. 2(b), the received signal for each code is compressed by the matched filter in the time domain, resulting in a very sharp correlation peak. Although the duration of $c_n(t)$, as illustrated in Fig. 2, is much longer than the relative delays between adjacent paths ($\tau_{n,l} - \tau_{n,l-1}$), the sharp autocorrelation peak of $c_n(t)$ results in a very fine multipath resolution of

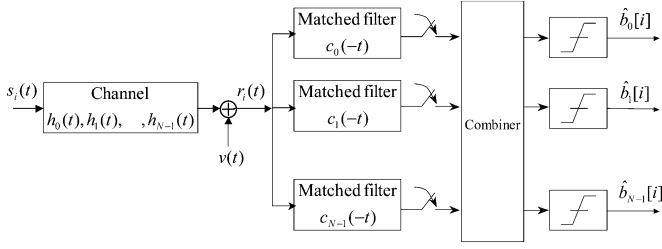


Fig. 5. Block diagram of the multicode receiver.

the receiver. Specifically, the proposed scheme has a multipath resolution that is approximately equal to the duration of the autocorrelation peak ($2/B_s$), i.e., any adjacent paths whose relative delays are greater than $2/B_s$ are resolvable. Apparently, a larger frequency-sweep range results in a finer multipath resolution. In order to capture multipath energy, however, a scheme to combine the resolvable paths is needed. This could be achieved by using the traditional rake-type receiver structures which consist of a bank of matched filters each matched to one of the transmitted codes. The detection process is illustrated in Fig. 5, where the outputs of each matched filter $c_0(-t), \dots, c_{N-1}(-t)$ are sampled according to the path delays $\tau_{n,l}$. The samples corresponding to the same code are combined for bit decision. Obviously, the chirp UWB system employing a rake receiver has the same energy capture problem as pulsed UWB systems.

The output signal of the filter matched to $c_n(t)$ can be expressed as

$$w_n(t) = \sum_{l=0}^{L-1} \sqrt{E_b} b_n [l] \alpha_{n,l} \phi_{n,n}(t - \tau_{n,l}) + \sum_{\substack{m=0 \\ m \neq n}}^{N-1} \sqrt{E_b} b_m [l] \sum_{l=0}^{L-1} \alpha_{m,l} \phi_{n,m}(t - \tau_{m,l}) + \xi(t) \quad (10)$$

where $\phi_{n,n}(t) = \int_{-\infty}^{\infty} c_n(\tau) c_n(t + \tau) d\tau = \int_{-T}^T c_n(\tau) c_n(t + \tau) d\tau$ is the autocorrelation² of $c_n(t)$, $\phi_{n,m}(t) = \int_{-T}^T c_n(\tau) c_m(t + \tau) d\tau$ is the cross-correlation function between $c_n(t)$ and $c_m(t)$, and $\xi(t) = \nu(t) * c_n(-t)$ ($*$ denotes convolution) is the filtered noise process. The second term on the right-hand side of (10) represents inter-code interferences. In an ideal Gaussian channel, $h_n(t) = \delta(t)$ and this term equals zero due to the orthogonality between $c_i(t)$ and $c_j(t)$ expressed in (5a). In a multipath channel, this term does not equal zero in general. Thus, it represents a small interference term due to the near-zero cross-correlation, as given in (5b), which has been illustrated in Fig. 3.

Ideally, the receiver could sample $w_n(t)$ at time instants corresponding to each path with delays $\tau_{n,l}$. For simplicity of notation, we will omit the frame index i in the following discussion.

The sampled value corresponding to the l th multipath component (sampled at $t = \tau_{n,l}$), noting that $\phi_{n,n}(0) = 1$, can be written as

$$w_{n,l} = \sqrt{E_b} b_n \alpha_{n,l} + \sqrt{E_b} \sum_{\substack{m=0 \\ m \neq n}}^{N-1} b_m \sum_{l=0}^{L-1} \alpha_{m,l} \phi_{n,m}(\tau_{n,l} - \tau_{m,l}) + \xi_{n,l} = \sqrt{E_b} b_n \alpha_{n,l} + I_{n,l} + \xi_{n,l} \quad (11)$$

where noise component $\xi_{n,l}$ has zero mean and variance $N_0/2$. The second term on the right-hand side of (11), the inter-code interference term, depends on the cross-correlation property of the codes. In the ideal case of perfect cross-correlation, $I_{n,l} = 0$. The samples corresponding to the L paths can be written in a vector form as

$$\mathbf{w}_n = [w_{n,0}, w_{n,1}, \dots, w_{n,L-1}]^T \quad (12)$$

where $(\cdot)^T$ denotes transpose. The decision variable for b_n is obtained by combining the elements of \mathbf{w}_n . The conventional method of maximal ratio combining (MRC) can be used, which results in a decision variable expressed as

$$\psi_n = \boldsymbol{\alpha}_n^T \mathbf{w}_n = \sqrt{E_b} b_n \sum_{l=0}^{L-1} \alpha_{n,l}^2 + \boldsymbol{\alpha}_n^T \mathbf{I}_n + \boldsymbol{\alpha}_n^T \boldsymbol{\xi}_n \quad (13)$$

where $\boldsymbol{\alpha}_n = [\alpha_{n,0}, \dots, \alpha_{n,N-1}]^T$, $\mathbf{I}_n = [I_{n,0}, \dots, I_{n,L-1}]^T$, and $\boldsymbol{\xi}_n = [\xi_{n,0}, \dots, \xi_{n,L-1}]^T$. For BPSK modulation, the n th bit of the i th frame can be detected by simply passing ψ_n through a decision device with a threshold "0."

III. ERROR PERFORMANCE IN INDOOR ENVIRONMENTS

Modeling the inter-code interference term $\boldsymbol{\alpha}_n^T \mathbf{I}_n$ given in (13) is generally difficult, as it depends on the cross-correlation values among the chirp codes. We derive the theoretical error performance assuming that $\phi_{n,m}(\tau_{n,l} - \tau_{m,n}) = 0, \forall m, n, l$. Thus, the result represents the lower bound to the performance in a real environment. For a carefully chosen set of time-domain spreading sequences \mathbf{a}_n , this bound could be very tight, which will be verified by simulation in Section IV. For a fixed set of fading coefficients $\{\alpha_{n,l}\}$, ψ_n is a Gaussian random variable (RV). Because the energy of $c_n(t)$ is normalized to unity, the instantaneous signal-to-noise ratio (SNR) per bit in the decision variable for bit b_n is obtained as

$$\gamma_b = \frac{2E_b}{N_0} \sum_{l=0}^{L-1} \alpha_{n,l}^2 = \sum_{l=0}^{L-1} \theta_{n,l} \quad (14)$$

where $\theta_{n,l} = (2E_b/N_0) \beta_{n,l}^2$ (note that $\alpha_{n,l} = \lambda_{n,l} \beta_{n,l}$ and $\lambda_{n,l} \in \{\pm 1\}$). Since $\alpha_{n,l}$ is a lognormal RV, $\theta_{n,l} = (2E_b/N_0) \beta_{n,l}^2$ is also a lognormal RV [21]. Thus, γ_b is a sum of independent lognormal RV's $\beta_{n,l}^2, l = 0, \dots, L-1$.

As in [22], we calculate the bit error rate (BER) for a fixed set of $\{\beta_{n,l}\}$ and then average the conditional BER over the probability density function (PDF) of γ_b . The conditional BER for a fixed set of $\{\beta_{n,l}\}$ is given as

$$p(\gamma_b) = \frac{1}{2} \operatorname{erfc} \left(\sqrt{\frac{\gamma_b}{2}} \right). \quad (15)$$

²To simplify notation, we have omitted the superscript in $\phi_{n,n}^{(c)}(t)$, which indicates that it is the autocorrelation of code $c_n(t)$.

Let $x_l = e^{y_l}$, where y_l is a normal RV, i.e., $y_l \sim N(\mu_{y_l}, \sigma_{y_l}^2)$. Then

$$\theta_l = e^{\epsilon_0 + 2y_l} \quad (16)$$

where $\epsilon_0 = \ln(E_b/N_0)$. The k th moment of x_l is given as

$$E\{x_l^k\} = e^{k\mu_{y_l} + k^2\sigma_{y_l}^2/2}. \quad (17)$$

Although an exact closed-form expression for the PDF of a sum of independent lognormal RVs does not exist, such a sum can be approximated by another lognormal RV. The approximation can be obtained by a number of methods, one of which is the Wilkinson's method [21], [23].

Let $\gamma_b = e^z$ where $z, z \sim N(\mu_z, \sigma_z^2)$, is a normal RV. In Wilkinson's method, the two parameters μ_z and σ_z are obtained by matching the first two moments of γ_b with the first two moments of $\sum_{l=0}^{L-1} \theta_{n,l}$. These two parameters are given as

$$\mu_z = \ln \left(\frac{E_{L1}^2}{\sqrt{E_{L2}}} \right) \quad (18a)$$

$$\sigma_z = \ln \left(\frac{E_{L2}}{E_{L1}^2} \right) \quad (18b)$$

where E_{L1} and E_{L2} are related to μ_{y_l} and $\sigma_{y_l}^2$ as

$$E_{L1} = \sum_{l=0}^{L-1} e^{(\epsilon_0 + 2\mu_{y_l} + 2\sigma_{y_l}^2)} \quad (19a)$$

$$E_{L2} = \sum_{l=0}^{L-1} e^{2(\epsilon_0 + 2\mu_{y_l} + 4\sigma_{y_l}^2)} + 2 \sum e^{2(\epsilon_0 + \mu_{y_m} + \mu_{y_n} + \sigma_{y_m}^2 + \sigma_{y_n}^2)} \quad (19b)$$

where the second sum in (19b) is extended to all combinations of (m, n) , $m < n = 0, \dots, L-1$.

The approximated PDF of γ_b is given as

$$f(\gamma_b) = \frac{1}{\gamma_b \sqrt{2\pi\sigma_z^2}} \exp \left[-\frac{(\ln(\gamma_b) - \mu_z)^2}{2\sigma_z^2} \right]. \quad (20)$$

The average BER can be calculated by averaging the conditional BER $p(\gamma_b)$ over $f(\gamma_b)$ as

$$P_b = \int_0^\infty p(\gamma_b) f(\gamma_b) d\gamma_b. \quad (21)$$

IV. NUMERICAL EXAMPLES

A. A Design Example

In this section, we provide an example of the proposed UWB signaling scheme using multicode chirp waveforms. The system parameters are summarized in Table I. For a channel with a root mean square (rms) delay spread of $\tau_{\text{rms}} = 15$ ns, the frequency separation between the two codes occupying adjacent bands is greater than the channel coherence bandwidth. Thus, all N codes will experience independent fading. Based on the design given in Table I, the maximum bit rate supportable by the eight quasi-orthogonal up-chirp codes using BPSK is 75 Mbps. Together with the eight quasi-orthogonal down-chirp codes, the aggregated throughput could be as high as 150 Mbps.

B. BER Results

The error performance of the design example given in Table I is simulated. We adopt the CM3 lognormal fading model [20]

TABLE I
SYSTEM PARAMETERS OF A DESIGN EXAMPLE

System Parameter	
Center frequency f_0	4.1 GHz
Total number of code waveforms N	8 up-chirp codes
Number of chips per code N_c	8
Chip duration T_c	16 ns
Code duration $T = N_c T_c$	128 ns
Chirp envelope for each chip $g(t)$	$\Pi(t/T)$
Instantaneous null-to-null bandwidth of $g(t)$ (B_c)	125 MHz
Total system bandwidth at any time when frequency sweep is stopped (NB_c)	1 GHz
Frequency-sweep range $B_s (= \mu T_c)$	1 GHz
Data modulation	BPSK
Detection	Coherent
Multipath combining	Maximal ratio combining

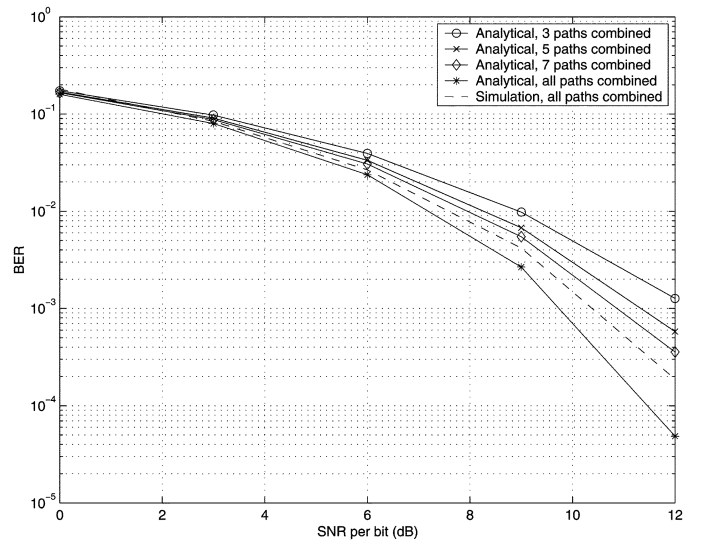


Fig. 6. Analytical and simulated error performance curves.

with an rms delay spread of 15 ns, an average cluster arrival rate of 0.0667/ns, and an average path arrival rate is 2.1/ns. The cluster decay factor applied is $\Gamma = 14$ ns, and the ray decay factor applied is $\gamma = 7.9$ ns. The standard deviation of the fading coefficients chosen is 3.4 dB. As the duration of code $c_n(t)$ (128 ns) is much greater than the channel rms delay spread, inter-symbol interference caused by channel excess delay given the bit rate of $1/T_b = 75$ Mb/s is negligible. Since the minimum separation between the center frequencies of any two codes $c_i(t)$ and $c_j(t)$ at any time instant is at least 125 MHz, which is greater than the channel coherence bandwidth (approximately equals a fraction of τ_{rms}^{-1}), channel coefficients for different codes are generated independently. The receiver is assumed to have perfect knowledge of the channel coefficients and delays.

Fig. 6 shows the analytical and simulated error performance curves of the example system. A total of 60 resolvable paths is considered, but the receiver may combine only a subset of them. Since the SNR per bit experienced by the receiver is used as the reference, the total energy from all paths combined by the receiver is normalized to unity. Note that if the energy of all paths available were normalized to unity, BER curves of receivers which combine only a subset of the available paths would have had an additional shift toward the right along the horizontal axis.

The analytical performance was obtained by using the method described in Section III. The analytical curve represents the performance lower bound, as the inter-code interference term in the decision variable given in (13) has been neglected. Simulation results are only provided for the case when all paths are combined and include the effect of intercode interference. By comparing the analytical and simulation results, it is found that the analytical lower bound is reasonably tight. When everything is ideal (no intercode and interpath interferences), performance of the proposed scheme is the same as the pulsed UWB employing a rake receiver.

V. CONCLUSION

We have proposed a multicode continuous-wave UWB signaling scheme that employs chirp waveforms. The construction of chirp codes, the data modulation scheme, and the receiver design have been discussed in detail. We have also analyzed the error performance of such a scheme in indoor lognormal fading environments. Compared with the pulsed UWB scheme, transmission in the proposed scheme is continuous in time. This approach avoids many of the hardware and implementation difficulties of pulsed UWB schemes while retaining the merits of pulsed schemes such as multipath diversity and accurate timing information. Additionally, the transmitter and matched filter receiver for the proposed scheme can be implemented using completely passive, low-cost, surface acoustic wave devices.

REFERENCES

- [1] "Revision of Part 15 of the Commission's Rules regarding ultra-wideband transmission systems," FCC notice of proposed rule making, ET-Docket 98-153.
- [2] R. Qiu, H. Liu, and X. S. Shen, "Ultra-wideband for multiple-access communications," *IEEE Commun. Mag.*, vol. 43, no. 2, pp. 80–87, Feb. 2005.
- [3] Z. Tian, L. Yang, and G. B. Giannakis, "Symbol timing estimation in ultra wide-band communications," in *Proc. 36th IEEE Asilomar Conf., Signals, Systems, Comput.*, Nov. 2002, pp. 1924–1928.
- [4] L. Zhao, A. M. Haimovich, and H. Grebel, "Performance of ultra-wideband communications in the presence of interference," in *Proc. IEEE Int. Conf. Commun.*, vol. 10, Jun. 2001, pp. 2948–2952.
- [5] I. Guvenc and H. Arslan, "Performance evaluation of UWB systems in the presence of timing jitter," in *Proc. IEEE UWBST*, Nov. 2003, pp. 136–141.
- [6] M. Z. Win and R. A. Scholtz, "On the robustness of ultra-wide bandwidth signals in dense multipath environments," *IEEE Commun. Lett.*, vol. 2, no. 2, pp. 51–53, Feb. 1998.
- [7] J. D. Choi and W. E. Stark, "Performance of ultra-wideband communications with suboptimal receiver in multipath channels," *IEEE J. Sel. Areas Commun.*, vol. 20, no. 10, pp. 1754–1766, Dec. 2002.
- [8] J. Balakrishnan, A. Batra, and A. Dabak, "A multiband OFDM system for UWB communication," in *Proc. 2003 IEEE Conf. Ultra-wideband Syst. Technol.*, Nov. 2003, pp. 354–358.
- [9] E. Saberinia and A. H. Tewfik, "Pulsed and nonpulsed OFDM ultra wide-band wireless personal area networks," in *Proc. IEEE UWBST*, Nov. 2003, pp. 275–279.

- [10] R. Qiu, "A study of the ultra-wideband wireless propagation channel and optimum UWB receiver design," *IEEE J. Sel. Areas Commun.*, vol. 20, no. 10, pp. 1628–1637, Dec. 2002.
- [11] H. G. Schantz, "Dispersion and UWB antennas," in *Proc. 2004 IEEE Int. Workshop Joint UWBST IWUWBS*, May 2004, pp. 161–165.
- [12] T. Yang, S.-Y. Suh, R. Nealy, W. A. Davis, and W. L. Stutzman, "Compact antennas for UWB applications," in *Proc. 2003 IEEE Conf. UWBST*, Nov. 2003, pp. 205–208.
- [13] G. Lu, P. Spasojevic, and L. Greenstein, "Antenna and pulse designs for meeting UWB spectrum density requirements," in *Proc. 2003 IEEE Conf. UWBST*, Nov. 2003, pp. 162–166.
- [14] K. Doi, T. Matsumura, K. Mizutani, and R. Kohno, "Ultra wide-band ranging system using improved chirp waveform," in *Proc. IEEE RAWCON*, Aug. 2003, pp. 207–210.
- [15] K. Doi, T. Matsumura, K. Mizutani, H. Tsuji, H. Wakana, S. Ohmori, and R. Kohno, "Frequency hopping ultra-wideband inter-vehicle radar system using chirp waveforms," in *Proc. 2004 Joint Int. Workshop UWBST IWUWBS*, May 2004, pp. 386–390.
- [16] R. Brocato, E. Heller, J. Wendt, J. Blaich, G. Wouters, E. Gurule, G. Omdahl, and D. Palmer, "UWB communication using SAW correlators," in *Proc. IEEE RAWCON*, Sep. 2004, pp. 267–270.
- [17] S. E. Carter and D. C. Malocha, "SAW device implementation of a weighted stepped chirp code signal for direct sequence spread spectrum communications systems," *IEEE Trans. Ultrasonics, Ferroelectrics, Frequency Control*, vol. 47, pp. 967–973, Jul. 2000.
- [18] A. Pohl, G. Ostermayer, L. Reindl, F. Seifert, and R. Weigel, "Fast adaptive interference cancellation in low cost SAW based chirp spread spectrum systems," in *Proc. 1998 IEEE Int. Symp. Spread Spectrum Techniques Applications*, 1988, pp. 883–887.
- [19] A. Springer, W. Gugler, M. Huemer, R. Koller, and R. Weigel, "A wireless spread-spectrum communication system using SAW chirped delay lines," *IEEE Trans. Microw. Theory Tech.*, vol. 49, pp. 754–760, Apr. 2001.
- [20] A. F. Molisch, J. R. Foerster, and M. Pendergrass, "Channel models for ultra-wideband personal area networks," *IEEE Wireless Commun.*, vol. 10, no. 6, pp. 14–21, Dec. 2003.
- [21] H. Liu, "Error performance of a pulse amplitude and position modulated ultra-wideband system in lognormal fading channels," *IEEE Commun. Lett.*, vol. 7, no. 11, pp. 531–533, Nov. 2003.
- [22] J. G. Proakis, *Digital Communications*, 3rd ed. New York: McGraw-Hill, 1995, ch. 14.
- [23] N. C. Beaulieu, A. A. Abu-Dayya, and P. J. McLane, "Estimating the distribution of a sum of independent lognormal random variable," *IEEE Trans. Commun.*, vol. 43, no. 12, pp. 2869–2873, Dec. 1995.



Huaping Liu (S'95–M'97) received the B.S. and M.S. degrees from Nanjing University of Posts and Telecommunications, Nanjing, China, in 1987 and 1990, respectively, and the Ph.D. degree from New Jersey Institute of Technology, Newark, in 1997, all in electrical engineering.

From July 1997 to August 2001, he was with Lucent Technologies, New Jersey. Since September 2001, he has been an Assistant Professor with the School of Electrical Engineering and Computer Science, Oregon State University, Corvallis. His

research interests include capacity and performance analysis of wireless systems, communication techniques for multiuser time-varying environments with applications to cellular and indoor wireless communications, ultra-wideband schemes, and MIMO-OFDM systems.